We are IntechOpen,
the world's leading publisher of
Open Access books
Built by scientists, for scientists

6,900
Open access books available

185,000
International authors and editors

200M
Downloads

154
Countries delivered to

Our authors are among the

TOP 1%
most cited scientists

12.2%
Contributors from top 500 universities

WEB OF SCIENCE™

Selection of our books indexed in the Book Citation Index
in Web of Science™ Core Collection (BKCI)

Interested in publishing with us?
Contact book.department@intechopen.com

Numbers displayed above are based on latest data collected.
For more information visit www.intechopen.com

Chaos Analysis and Control in AFM and MEMS Resonators

Amir Hossein Davaie-Markazi and Hossein Sohanian-Haghighi
School of Mechanical Engineering, Iran University of Science and Technology,
Tehran,
Iran

1. Introduction

For years, chaotic phenomena have been mainly studied from a theoretical point of view. In the last two decades, considerable developments have occurred in the control, prediction and observation of chaotic behaviour in a wide variety of dynamical systems, and a large number of applications have been discovered and reported (Moon & Holmes, 1999; Endo & Chua, 1991; Kennedy, 1993). Chaotic behaviour can only be observed in particular nonlinear dynamical systems. In recent years, nonlinearity is known as a key characteristic of micro resonant systems. Such devices are used widely in variety of applications, including sensing, signal processing, filtering and timing. In many of these applications some purely electrical components can be replaced by micro mechanical resonators. The benefits of using micro mechanical resonators include smaller size, lower damping, and improved the performance. Two examples of micro mechanical resonators that their complex behaviour is described briefly in this chapter are atomic force microscopy (AFM) and micro electromechanical resonators. AFM has been widely used for surface inspection with nanometer resolution in engineering applications and fundamental research since the time of its invention in 1986 (Hansma et al., 1988). The mechanism of AFM basically depends on the interaction of a micro cantilever with surface forces. The tip of the micro cantilever interacts with the surface through a surface–tip interaction potential. One of the performance modes of an AFM is the so called "tapping mode". In this mode, the micro-cantilever is driven to oscillate near its resonance frequency, by a small piezoelectric element mounted in the cantilever. In this chapter it will be shown that micro-cantilever in tapping mode may exhibit chaotic behaviour under certain conditions. Such a chaotic behaviour has been studied by many researchers (Burnham et al. 1995; Basso et al., 1998; Ashhab et al., 1999; Jamitzky et al., 2006; Yagasaki, 2007).

In section 3, the chaotic behaviour of micro electromechanical resonators is studied. Micro electromechanical resonant systems have been rapidly growing over recent years because of their high accuracy, sensibility and resolution (Bao, 1996). The resonators sensing application concentrate on detecting a resonance frequency shift due to an external perturbation such as accreted mass (Cimall et al., 2007). The other important technological applications of mechanical resonators include radiofrequency filter design (Lin et al., 2002) and scanned probe microscopy (Garcia et al., 1999). Many researchers have tried to analyze nonlinear behaviour in micro electeromechanical systems (MEMS) (Mestrom et al., 2007;

Younis & Nayfeh, 2003; Braghin et al., 2007). We will examine the mathematical model of a micro beam resonator, excited between two parallel electrodes. Chaotic behaviour of this model is studied. A robust adaptive fuzzy method is introduced and used to control the chaotic motion of micro electromechanical resonators.

2. Atomic force microscopy

The mechanism of an AFM basically depends on the interaction of a micro cantilever with surface forces. The tip of the micro cantilever interacts with the surface through a surface–tip interaction potential. One of the performance modes of an AFM is the so called "tapping mode". In this mode, the micro-cantilever is driven to oscillate near its resonance frequency, by a small piezoelectric element mounted in the cantilever. When the tip comes close to an under scan surface, particular interaction forces, such as Van der Waals, dipole-dipole and electrostatic forces, will act on the cantilever tip. Such interactions will cause a decrease in the amplitude of the tip oscillation. A piezoelectric servo mechanism, acting on the base structure of the cantilever, controls the height of the cantilever above the sample so that the amplitude of oscillation will remain close to a prescribed value. A tapping AFM image is therefore produced by recording the control effort applied by the base piezoelectric servo as the surface is scanned by the tip.

From theoretical investigations it is known that the nonlinear interaction with the sample can lead to chaotic dynamics although the system behaves regularly for a large set of parameters. In this section, the model of micro cantilever sample interaction is described and dynamical behaviour of forced system is investigated. The cantilever tip sample interaction is modelled by a sphere of radius R and equivalent mass m which is connected to a spring of stiffness k. A schematic of the model is shown in Fig.1. The interaction of an intermolecular pair is given by the Lennard Jones potential which can be modelled as (Ashhab et al., 1999)

$$V(x,Z) = -\frac{A_2 R}{6(Z+x)} + \frac{A_1 R}{1260(Z+x)^7} \tag{1}$$

where A_1 and A_2 are the Hamaker constants for the attractive and repulsive potentials. To facilitate the study of the qualitative behaviour of the system, the following parameters are defined:
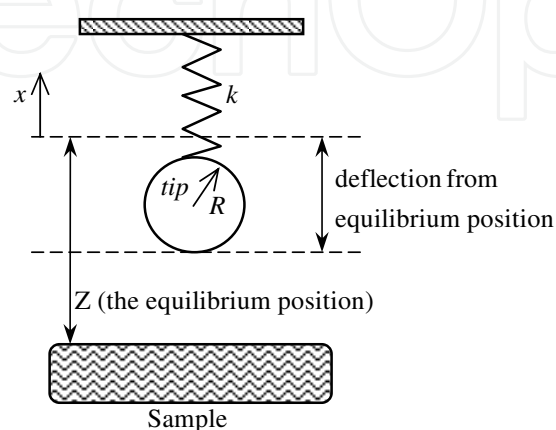

Fig. 1. The tip sample model.

$$D = \frac{A_2 R}{6k}, \; Z_s = \frac{3}{2}(2D)^{\frac{1}{3}}, \; \alpha_0 = \frac{Z}{Z_s}, \; d_0 = \frac{4}{27}, \; \Sigma = \left(\frac{A_1}{A_2}\right)^{\frac{1}{6}} \frac{1}{Z_s}, \; \zeta_1 = \frac{x}{Z_s}, \; \zeta_2 = \dot{\zeta}_1, \; \omega = \sqrt{\frac{k}{m}}, \; \tau = \omega t \; (2)$$

where t denotes time and the dot represents derivative with respect τ.

Using these parameters, the cantilever equation of motion with air damping effect, is described in state space as below

$$\begin{aligned}
\dot{\zeta}_1 &= \zeta_2 \\
\dot{\zeta}_2 &= -\zeta_1 - \delta\zeta_2 - \frac{d_0}{(\alpha_0 + \zeta_1)^2} + \frac{\Sigma^6 d_0}{30(\alpha_0 + \zeta_1)^8} + \Gamma\cos\Omega\tau
\end{aligned} \quad (3)$$

where δ is the damping factor and Γ and Ω are the amplitude and frequency of driving force respectively. Fig.2 shows a qualitative phase portrait of unforced system. There are two homoclinic trajectories each one connected to itself at the saddle point.
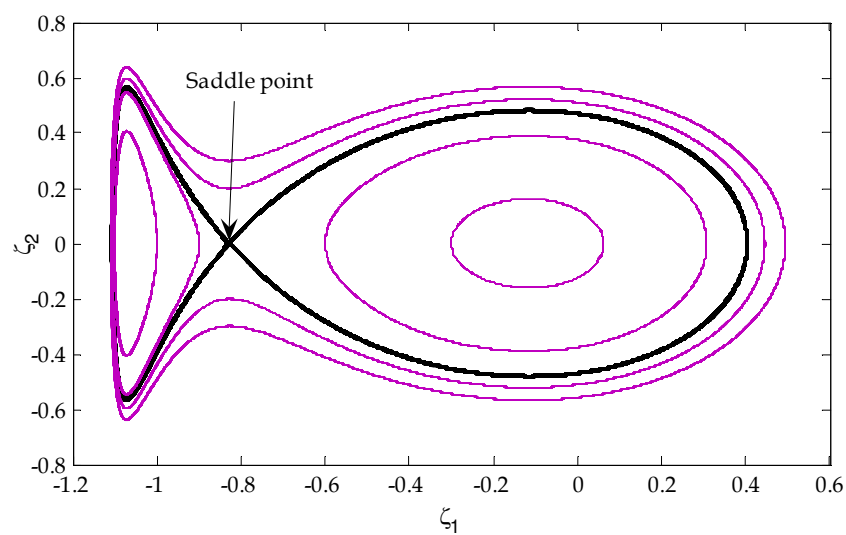

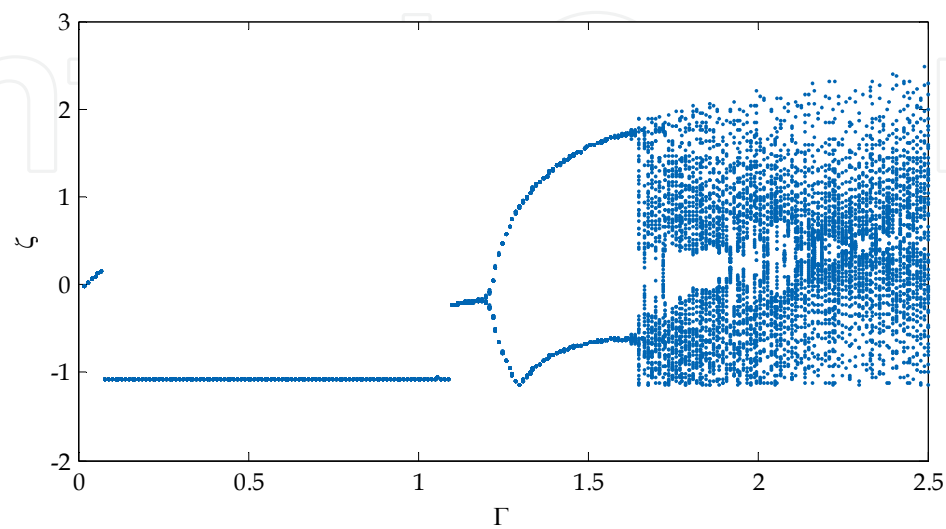Fig. 2. Phase diagram for unforced AFM model.

Fig. 3. The bifurcation diagram obtained by varying Γ from 0 to 2.5.

For numerical simulation, we consider (3), where the parameters have been set as follows: $\Sigma = 0.3$, $\alpha = 1.25$, $\delta = 0.05$, $\Omega = 1$. For these values, the bifurcation diagram of AFM model is shown in Fig. 3, where the parameter Γ is plotted versus the cantilever tip positions in the corresponding Poincare map. The obtained diagram reveals that, starting at $\Gamma = 1.2$, the period orbit undergoes a sequence of period doubling bifurcation. For the range $\Gamma \in (1.7, 2.5)$, the system shows complex behaviours. Fig. 4 shows various types of system responses for $\Gamma = 1$, $\Gamma = 1.5$ and $\Gamma = 2$.

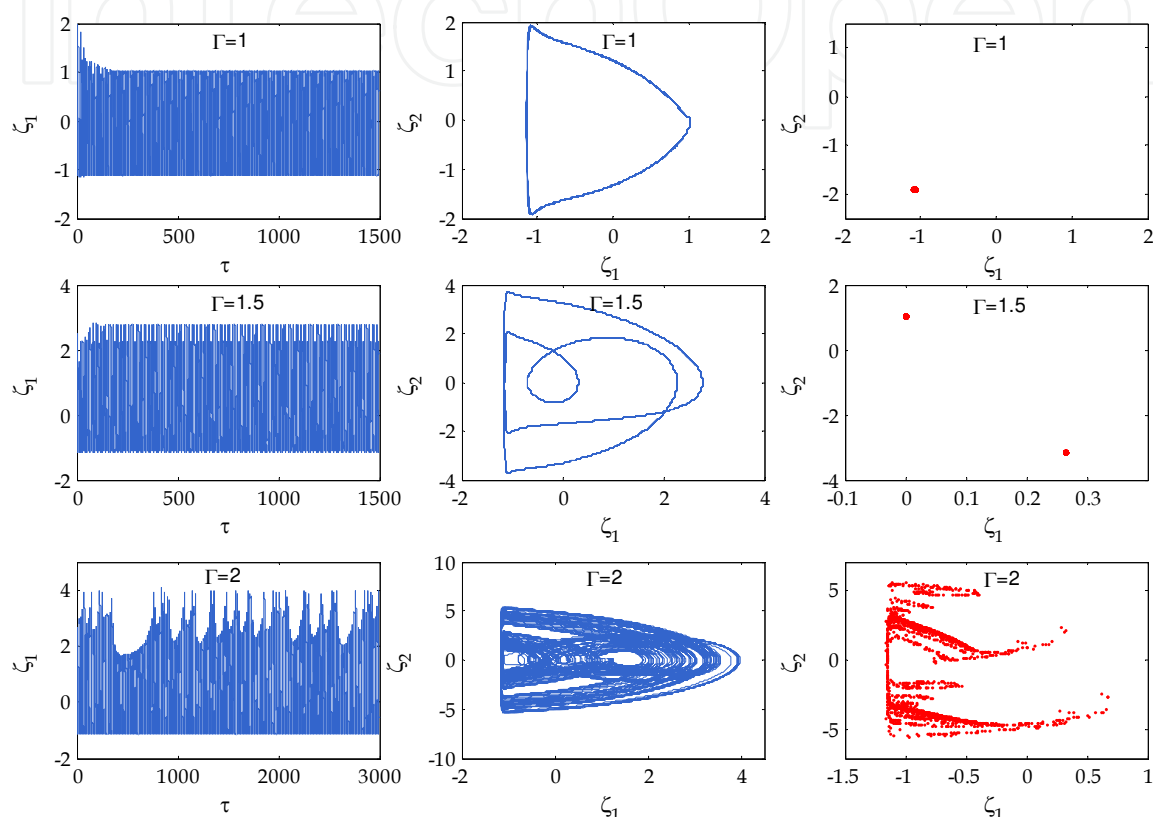Fig. 4. Time histories, corresponding phase diagrams and Poincare maps obtained by simulating (3).

3. Micro electromechanical resonators

In many cases it is highly desirable to reduce the size of MEMS mechanical elements (Roukes, 2001). This allows increasing the frequencies of mechanical resonances and improving their sensitivity as sensors. Although miniaturized MEMS resonant systems have many attractions, they also provide several important challenges. A main practical issue is to achieve higher output energy, in particular, in devices such as resonators and micro-sensors. A common solution to the problem is the well-known electrostatic comb-drive (Xie & Fedder, 2002). However, this solution adds new constraints to the design of the mechanical structure due to the many complex and undesirable dynamical behaviours associated with it. Another way to face this challenge is to use a strong exciting force (Logeeswaran et al., 2002; Harley, 1998). The major drawback of this approach is the nonlinear effect of the electrostatic force. When a beam is oscillating between parallel electrodes, the change in the capacitance is not a perfectly linear function. The forces

attempting to restore the beam to its neutral position vary as the beam bends; the more the beam is deflected, the more nonlinearity can be observed. In fact nonlinearities in MEMS resonators generally arise from two distinct sources: relatively large structural deformations and displacement-dependent excitations. Further increasing in the magnitude of the excitation force will result in nonlinear vibrations, which will affect the dynamic behavior of the resonator, and may lead to chaotic behaviors (Wang et al., 1998). The chaotic motion of MEMS resonant systems in the vicinity of specific resonant separatrix is investigated based on the corresponding resonant condition (Luo & Wang., 2002). The chaotic behavior of a micro-electromechanical oscillator was modelled by a version of the Mathieu equation and investigated both numerically and experimentally in (Barry et al., 2007). Chaotic motion was also reported for a micro electro mechanical cantilever beam under both open and close loop control (Liu et al., 2004).

In this section, the chaotic dynamics of a micro mechanical resonator with electrostatic forces on both upper and lower sides of the cantilever is investigated. Numerical studies including phase portrait, Poincare map and bifurcation diagrams reveal the effects of the excitation amplitude, bias voltage and excitation frequency on the system transition to chaos. Moreover a robust adaptive fuzzy control algorithm is introduced and applied for controlling the chaotic motion. Additional numerical simulations show the effectiveness of the proposed control approach.

3.1 Mathematical model

An electrostatically actuated microbeam is shown in Fig.5. The external driving force on the resonator is applied via an electrical driving voltage that causes electrostatic excitation with a dc-bias voltage between electrodes and the resonator: $V_i = V_b + V_{AC} Sin\Omega t$, where, V_b is the bias voltage, and V_{AC} and Ω are the AC amplitude and frequency, respectively. The net actuation force, F_{act}, can then be expressed as (Mestrom et al., 2007)

$$F_{act} = \frac{1}{2}\frac{C_0 d}{(d-z)^2}(V_b + V_{AC} Sin\Omega t)^2 - \frac{1}{2}\frac{C_0 d}{(d+z)^2}(V_b^2)$$

(4)

where C_0 is the capacitance of the parallel-plate actuator at rest, d is the initial gap width and z is the vertical displacement of the beam. The governing equation of motion for the dynamics of the MEMS resonator can be expressed as
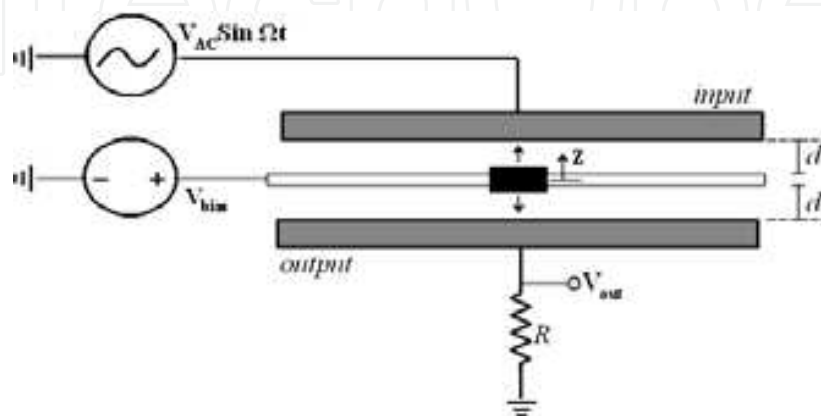

Fig. 5. A schematic picture of the electrostatically actuated micromechanical resonator.

$$m_{eff}z'' + bz' + k_1z + k_3z^3 = F_{act} \tag{5}$$

where, z' and z'' represent the first and second time derivative of z, and m_{eff}, b, k_1 and k_3 are effective lumped mass, damping coefficient, linear mechanical stiffness and cubic mechanical stiffness of the system respectively.

It is convenient to introduce the following dimensionless variables:

$$\tau = \omega_0 t, \ \omega = \frac{\Omega}{\omega_0}, x = \frac{z}{d}, \mu = \frac{b}{m_{eff}\omega_0}, \alpha = \frac{k_1}{m_{eff}\omega_0^2}, \beta = \frac{k_3d^2}{m_{eff}\omega_0^2}, \gamma = \frac{C_0V_b^2}{2m_{eff}\omega_0^2d^2}, A = 2\gamma\frac{V_{AC}}{V_b} \tag{6}$$

where ω_0 is the purely elastic natural frequency defined as

$$\omega_0 = \sqrt{\frac{k_1}{m_{eff}}} \tag{7}$$

Assuming the amplitude of the AC driving voltage to be much smaller than the bias voltage, with the dimensionless quantities defined in (6) the nondimensional equation of motion is obtained:

$$\ddot{x} + \mu\dot{x} + \alpha x + \beta x^3 = \gamma\left(\frac{1}{(1-x)^2} - \frac{1}{(1+x)^2}\right) + \frac{A}{(1-x)^2}Sin\omega\tau \tag{8}$$

Here, the new derivative operator, ($\cdot$), denotes the derivative with respect to τ. It is worth mentioning that, if the potential is set to be zero at $x = 0$, the corresponding potential can be described as

$$V(x) = \frac{\alpha x^2}{2} + \frac{\beta x^4}{4} - \gamma\left(\frac{1}{1-x} + \frac{1}{1+x}\right) + 2\gamma \tag{9}$$

Fig. 6 shows that the change in the number of equilibrium points, when the applied voltage is changed. For the case where the bias voltage does not exist, only one stable state exists,
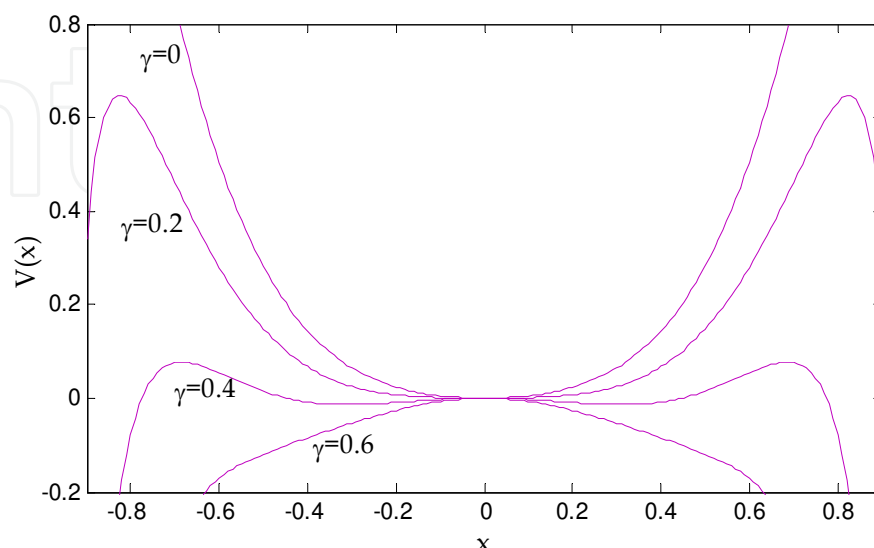

Fig. 6. The potential function for four values of γ ($\gamma = 0, 0.2, 0.4, 0.6$), $\alpha = 1$ and $\beta = 10$.

and the equilibrium point is a stable center point at x=0. When the bias voltage is not zero, however, at a critical position, the resonator becomes unstable and is deflected against one of the stationary transducer electrodes (pull-in phenomena). If the bias is small, the structure stays in the deflected position, smaller than the critical one. For this case, three associated equilibrium points are one stable center point and two unstable saddle points. As the bias voltage increases, the equilibrium point at x=0 becomes unstable and the potential function V(x) will have a local peak at this point. The original equilibrium point at the center position becomes a saddle point and two new center points emerge at either side of the origin. For a large enough bias voltage, there is only one unstable equilibrium point at x=0 and the resonator becomes completely unstable.

3.2 Transition to chaos

To verify the analytical findings, a series of numerical simulations of the exact nonlinear differential equation (5) is performed with the following dimensionless parameters:

$m = 5 \times 10^{-12} kg, \ b = 5 \times 10^{-8} kg/s, \ k_1 = 5 \mu N/\mu m, \ k_3 = 15 \mu N/\mu m^3, \ d = 2 \mu m, \ C_0 = 1.5 \times 10^{-14} F,$

$V_b = 30V, \omega = 0.5.$

The unforced system has a saddle point at $x = 0$ as can be seen from Fig. 7. Existence of this point makes homoclinic bifurcations to take place possible. This means that the system has the necessary condition for chaotic behaviour.

The phase portrait and time histories are plotted for different values of the AC voltage. To study the effect of the AC voltage on the beam dynamics, the bias voltage is kept fix and the AC voltage is varied. Starting from the vicinity of the critical amplitude for $V_{AC} = 0.06V$, the system response contains transient chaos and periodic motion around one of the center points (Fig. 8a). Fig. 8b reveals that following the transient chaos, the beam oscillates in the vicinity of the other center point for $V_{AC} = 0.17V$. The more increase in the AC voltage causes a longer transient chaotic motion. The chaotic transient oscillation is large in amplitude and jumping between potential wells. After a while in such a regime of motion, a steady state regular vibration with much smaller amplitude, and located in a single potential well, is observed. As can be seen from Fig. 8c, after the transient chaotic response, a periodic motion may be observed, evolving out of the homoclinic orbit and, with much larger
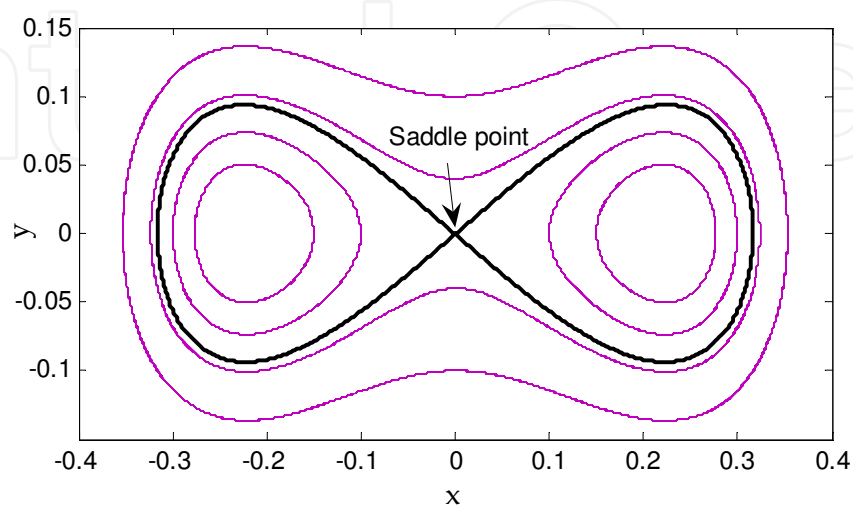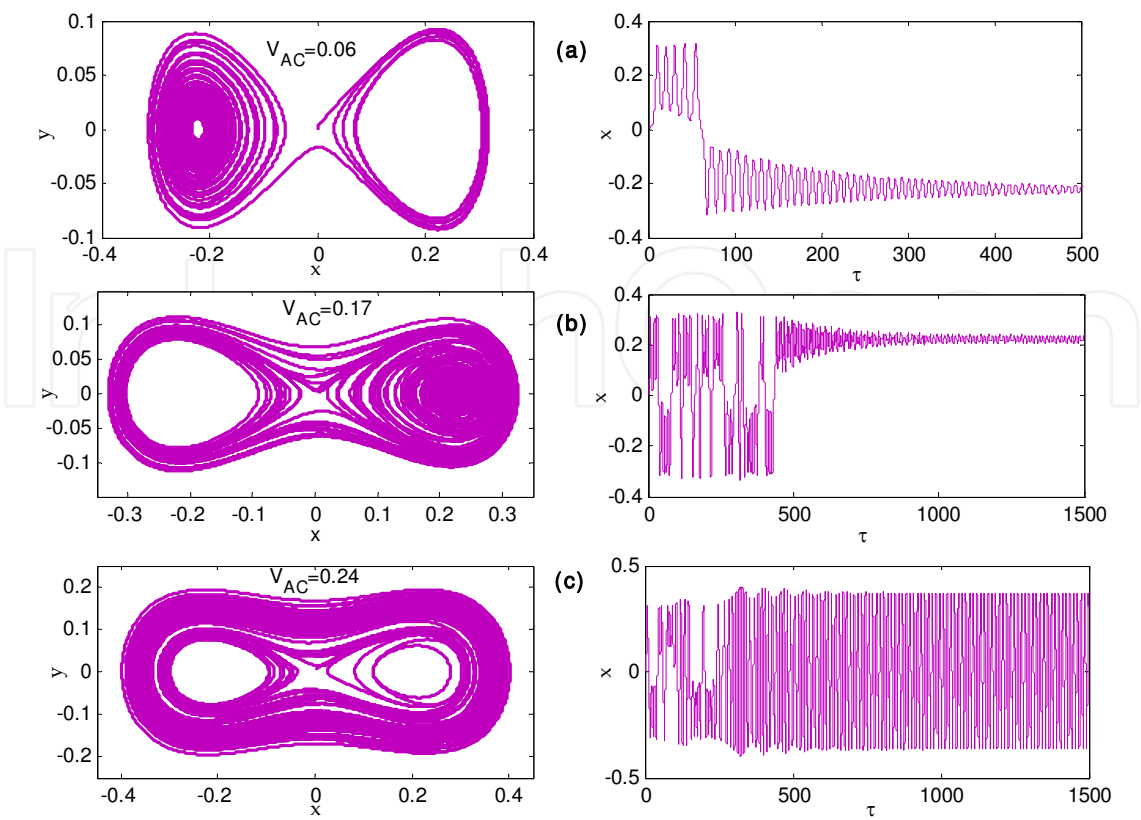

Fig. 7. Phase portraits of unforced system.

Fig. 8. Phase diagrams and time histories obtained by simulating (5). Corresponding AC voltages are indicated in phase diagrams.

amplitude. ($V_{AC} = 0.24V$). With a large enough stimulation time, the system is brought back to chaotic steady state. Fig.9 shows the phase trajectory and the Poincare map of the chaotic motion, with $V_{AC} = 1.8V$. The system behavior is different from that of the Duffing attractor because of the electrostatic terms in the MEMS equations. Because of the two unstable points near the fixed electrodes, there is an upper limit for the applied AC voltage.
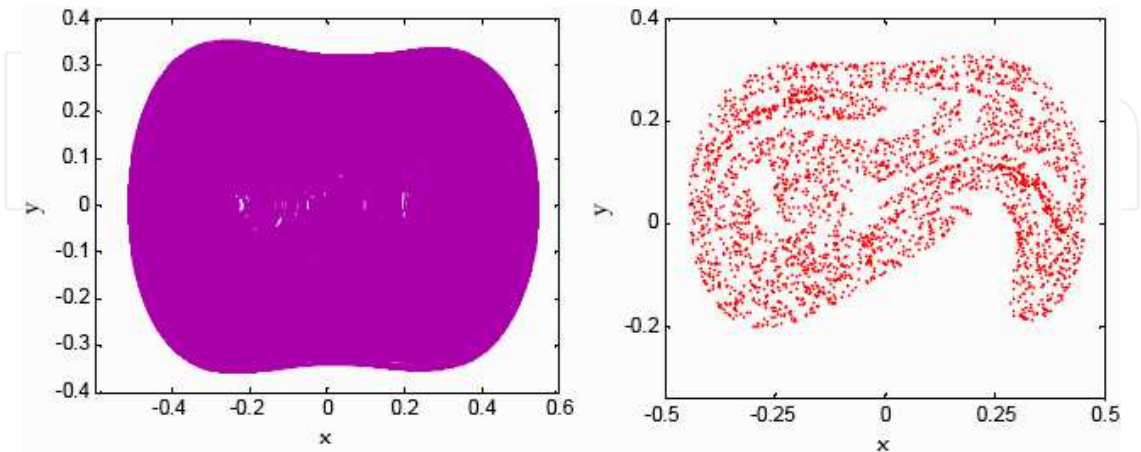

Fig. 9. The phase trajectory and the Poincare map when $V_{AC} = 1.8V$.

Any more increase in the AC voltage, leads to a dynamic pull-in phenomena, which could to instability at a voltage lower than the static pull-in voltage. In interpreting the results in

Fig. 10, note that $V_{AC} = 2.8V$ corresponds to collapse of the microbeam into the fixed electrode.
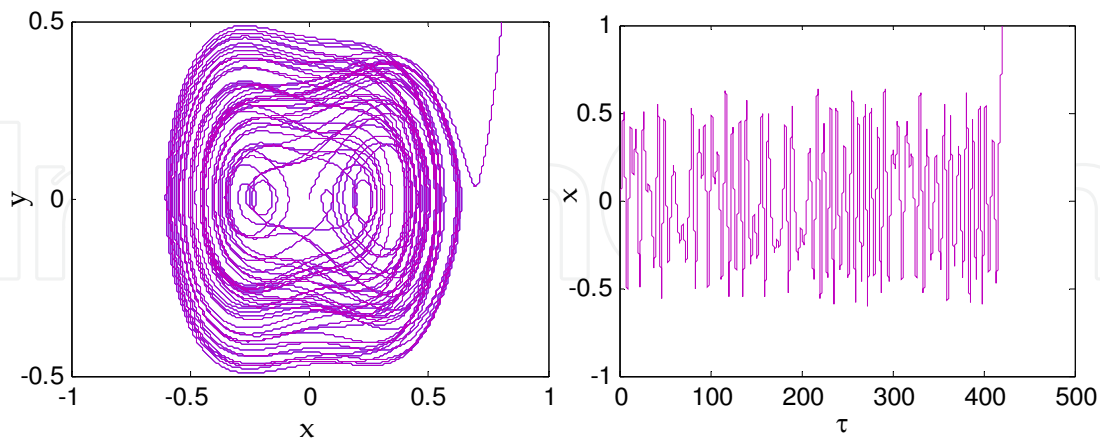

Fig. 10. The phase trajectory and time history for x(t) obtained with $V_{AC} = 2.8V$.

3.3 Bifurcation diagrams

Fig.11 shows the bifurcation diagram. In this case, the qualitative behavior of the system is shown against a varying AC voltage from 0 to 2.8. In the bifurcation diagram, the final system states of the previously iterated value of the AC voltage is chosen as the initial condition for the next system iteration with the new value of the AC voltage. Chaotic behavior of system starts when $V_{AC} = 1.4V$ and continues until $V_{AC} = 2.8V$. For AC voltages larger than 2.8V, the dynamic pull-in may occur, where, the electric force increases and becomes much higher than the spring restoring force and the resonator sticks to one of the stationary electrodes (Nayfeh &Younis, 2007). The initial conditions are assumed as $(x_{in}, v_{in}) = (0,0)$ for all simulation studies.
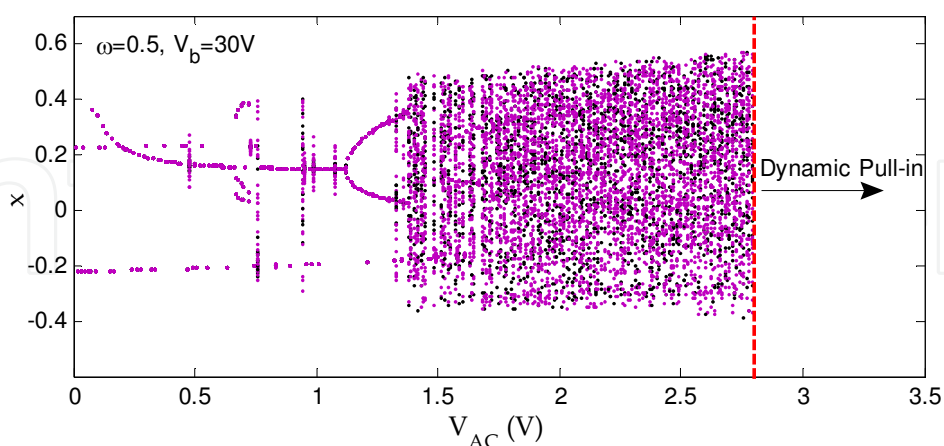

Fig. 11. The bifurcation diagram obtained by varying AC voltage from 0 to 2.8V.

The characteristic dynamical behaviors are investigated by varying the bias voltage. Fig.12 shows the bifurcation diagram of the micro beam displacement via the applied bias voltage. The figure indicates that, with an increase in the applied bias voltage, a period-doubling bifurcation occurs, i.e., a period-1 motion becomes a period-2 motion. If the applied bias

voltage is increased, a chaotic behavoir may occur. The figure demonstrates that the chaotic region becomes wider as the applied bias voltage is increased.
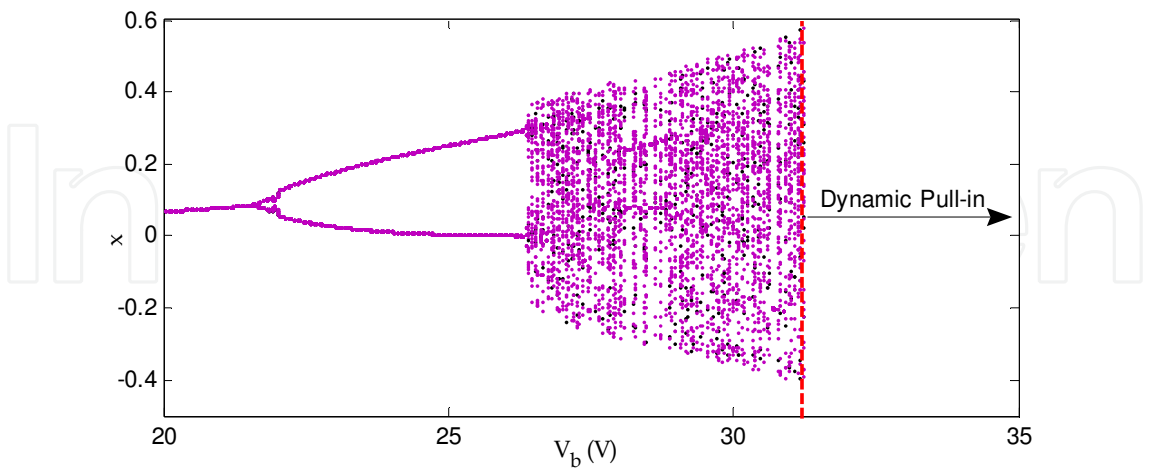

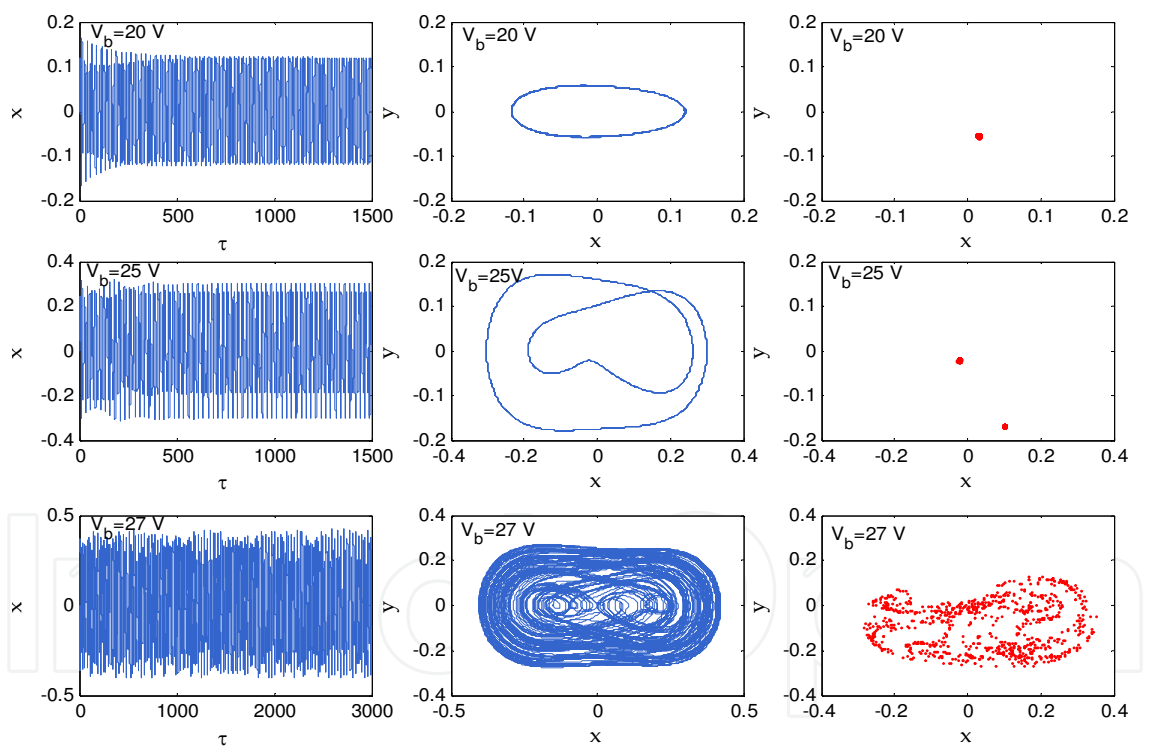Fig. 12. The bifurcation diagram obtained by varying the bias voltage from 20 to 32V.

Fig. 13. Time histories and corresponding phase diagrams and Poincare maps obtained by simulating (5) with $\omega = 0.5$ and $V_{AC} = 1.8V$.

It can be seen from Fig. 13, that the system responses contain periodic and chaotic motions. When $V_b = 20V$, the vibration amplitude of the cantilever is small, the period-1 motion with only one isolated point in Poincare map and one circle in phase portrait can be observed. With an increase in the amplitude of the applied bias voltage, the motion becomes synchronous with period-two, as illustrated in Fig. 13 for $V_b = 25V$. Moreover, at $V_b = 27V$,

the micro beam displacement response becomes chaotic and no regular pattern can be observed in the corresponding Poincare map and the phase portrait.
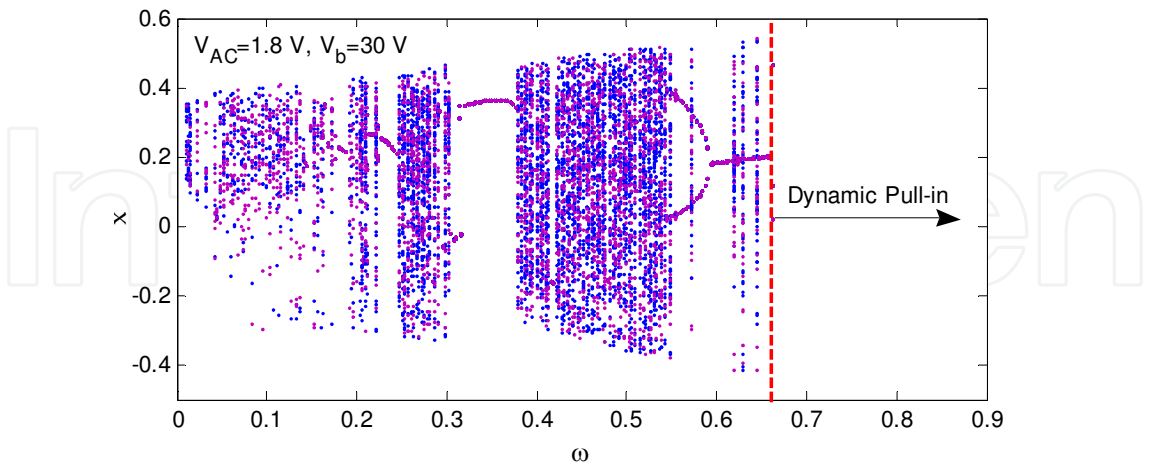

Fig. 14. The bifurcation diagram obtained by varying ω from 0 to 0.67.

Fig. 14 shows that the system responses exhibit an alternation of periodic and chaotic motions. The system response comes into a steady-state synchronous motion with period-1, and returns to the chaotic motion alternatively, as the excitation frequency is increased. Period-doubling motions are also observed for a small range of excitation frequencies.
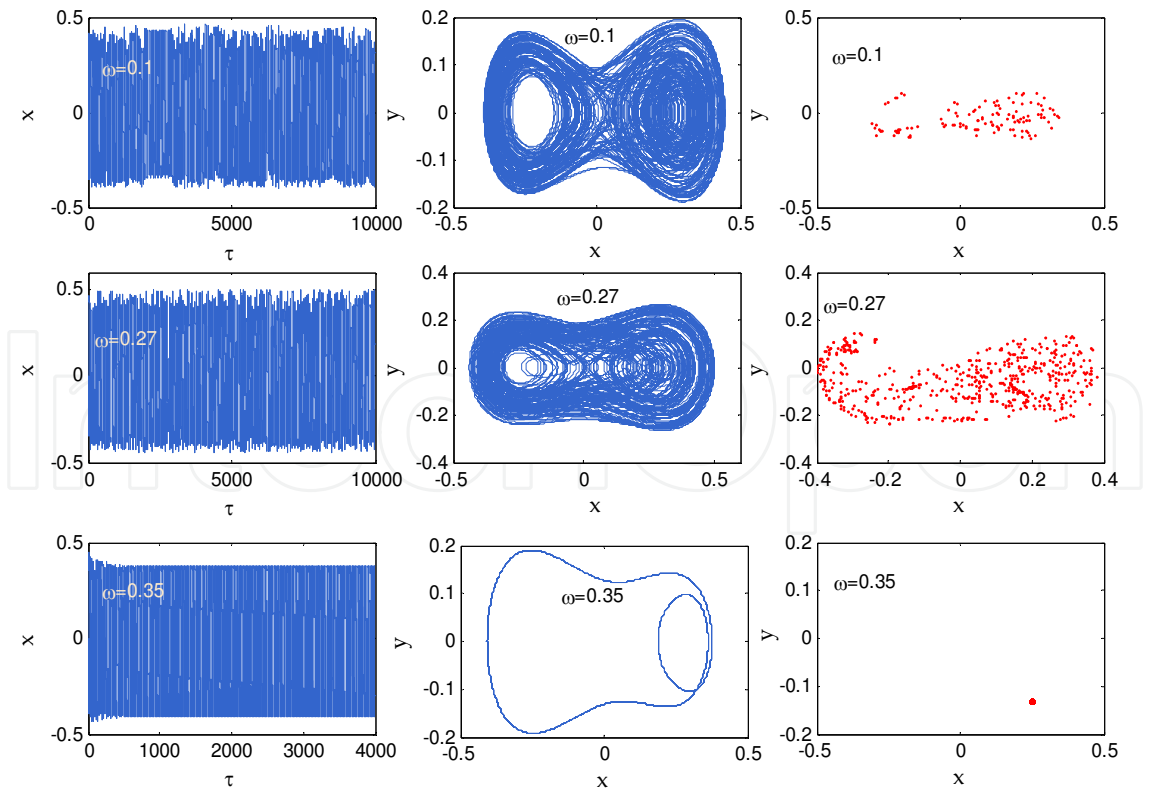

Fig. 15. Time histories, corresponding phase diagrams and Poincare maps obtained by simulating (5) with $V_b = 30V$ and $V_{AC} = 1.8V$.

Fig. 15 depicts the time history, phase plane portraits and the Poincare maps based on the responses of the electrostatically actuated system over a range of frequencies. Various chaotic behavior is observed for $\omega = 0.2$ and $\omega = 0.27$. It can be seen that, for $\omega = 0.35$, the motion of the system is synchronized with period-one.

3.4 Control of chaotic motion in MEMS resonator

Various fuzzy control methods for control of chaotic systems are proposed in the literature e.g., (Calvo, 1998; Poursamad & Markazi, 2009-a; Haghighi & Markazi, 2010). In this section, a robust adaptive fuzzy control algorithm is used to stabilize a MEMS beam in a high-amplitude oscillation state. A key issue that arises in chaos control, particularly in MEMS resonators, is that the system parameters are not known precisely, and are perturbed during operation (Wang et al., 1998). Unlike most conventional control systems whose equilibriums are assumed known and fixed regardless of values of the system parameters, the equilibriums of chaotic systems are a function of their system constant parameters. This suggests that, when the system parameters are not precisely known, and hence, the equilibriums are then unknown, the conventional control methodologies may not be applied directly. In addition, the presence of external disturbance and measurement noise, may adversely affect the system performance. Therefore, development of alternative control strategies for efficient control and robust tracking of chaotic systems, under the presence of uncertainties is highly desirable.

The controller proposed in this section comprises a fuzzy system and a robust controller. The fuzzy system, whose parameters are adaptively tuned, is designed based on the sliding-mode control (SMC) strategy to mimic the ideal controller, i.e., when the model of the plant is exactly known. The robust controller is then designed to compensate for deviations of the fuzzy controller, compared to the ideal one. The uncertainty bound needed in the robust controller is also adaptively tuned online to avoid using unnecessary high switching gain, due to the, most often, conservative bounds. A comprehensive presentation of the proposed control method and proof of the asymptotic stability can be found in (Poursamad & Markazi, 2009-a ; Poursamad & Markazi, 2009-b).

In order to write (5) in a more convenient form, it is rewritten as

$$\ddot{x} = f(\dot{x}, x, t) + u \,, \tag{10}$$

where u is the appended control input and f is a smooth function obtained from (5). Now let define a sliding surface, $S(t)$, using $s(\dot{\tilde{x}}, \tilde{x}) = 0$ with $s(\dot{\tilde{x}}, \tilde{x}) = \dot{\tilde{x}} + \lambda \tilde{x}$, where $\tilde{x} = x_d - x$ is the tracking error, $\dot{\tilde{x}}$ is the time derivative of $\tilde{x}$, x_d is the desired trajectory and λ is a to be selected strictly positive constant. Now, an ideal (central) control signal is obtained as

$$u^* = -f + \ddot{x}_d + \lambda \dot{\tilde{x}} \tag{11}$$

and the control law is defined as

$$u = u^* + u_{rb} \,, \tag{12}$$

where, the robust control signal, u_{rb}, is designed to overcome the deviations from the sliding surface, by employing a switching strategy:

$$u_{rb} = \delta \operatorname{sgn}(s) \tag{13}$$

Here, δ is the bound of uncertainties. It is noted that, in the design of a conventional SMC, the uncertainty bound δ, must be known or estimated at the outset of the control design, a matter which is not easily achievable in practice. Such uncertainties may include unknown plant dynamics, parameter variations, and external load disturbances. In particular, the dynamics of micro/nano electromechanical systems are not known exactly, so the ideal controller proposed in (11) may not actually work in practice. As an alternative, the ideal controller can be approximated by a fuzzy inference system

$$u^* = \hat{B}^T W(s) + \psi \tag{14}$$

Here, $\hat{B}$ is the estimated value for the optimal weighting vector, and $W = \begin{bmatrix} w_1 & \cdots & w_n \end{bmatrix}^T$ is a vector with components $w_r(s) = \mu_r / \sum_{r=1}^{n} \mu_r$ and, where, μ_r is the firing strength of the rth rule of the fuzzy algorithm. The bias term ψ represents unmodeled dynamics and external disturbances and is assumed to be bounded as $|\psi| \le \psi$. The weighting vector can be updated by the adaptation rule $\dot{\hat{B}} = \alpha_1 s(t) W$, and the bound of uncertainties is estimated by the adaptation rule $\dot{\psi} = \alpha_2 |s(t)|$, where α_1 and α_2 are strictly positive constants, adaptation rates.
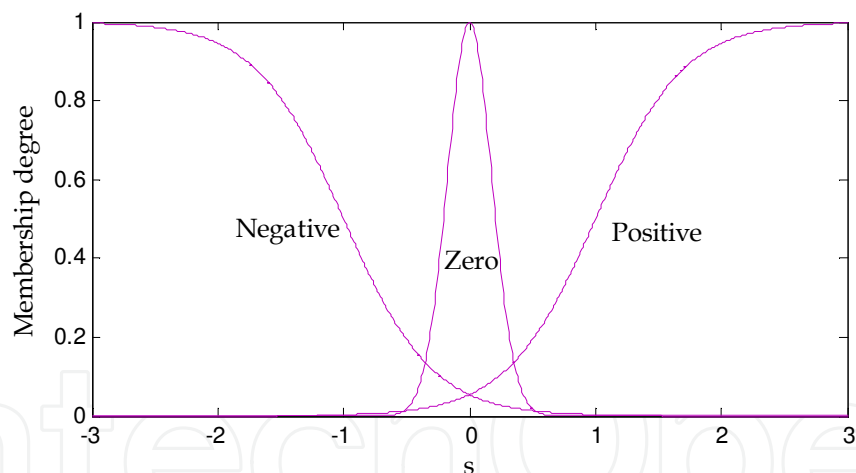

Fig. 16. Membership functions of s for robust adaptive fuzzy control.

The objective is to control the position variable x so as to track the desired trajectory $x_d = 0.6 \sin 0.5\tau$. The resonator properties are the same as introduced in Section 3.2 and $V_{AC} = 1.8V$. The input membership functions are selected as shown in Fig. 16 and the sliding surface is defined as $s = \dot{\tilde{x}} + \tilde{x}$. The parameters of these membership functions are chosen such that the parameter s remains close to zero. The initial weighting vector is arbitrarily selected as $\hat{B} = \begin{bmatrix} 1 & 0 & 1 \end{bmatrix}^T$, the initial value of the uncertainty bound is chosen as $\psi = 0.01$ and the learning rates are set to $\alpha_1 = 1$ and $\alpha_2 = 2 \times 10^{-4}$. The controller is activated at $\tau = 200$, for which the resulting output is depicted in Fig. 17, showing the effectiveness of the proposed control strategy.
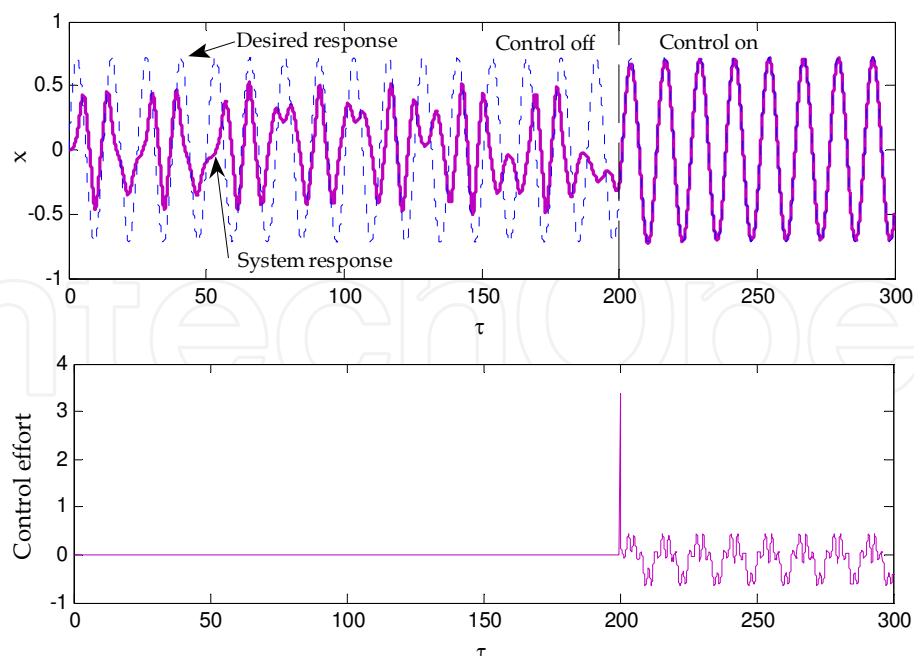
Fig. 17. Simulation results for MEMS resonator with proposed control strategy.

4. Conclusions

This chapter deals with the chaotic motion of micromechanical resonators. The source of nonlinearities in AFM is the Lennard Jones force while nonlinearities in MEMS resonator system include mechanical nonlinearity due to large deformation and nonlinear electrostatic forces. It is shown that each of these systems has one unstable fix point that connects the corresponding homoclinic trajectory to itself. Certain set of parameters may cause homoclinic bifurcation in these systems. Such a bifurcation corresponds to double periodic behavior of the system. It is seen that increase in the amplitude of driving force could lead to a chaotic motion. Finally, an adaptive fuzzy-sliding mode strategy was proposed for control of the chaotic motion. It was shown through simulations study that such a control strategy could successfully eliminate the chaotic motion and force the system response towards a stable orbit.

5. References

Ashhab, M. ; Salapaka, M.V.; Dahleh, M. & Mezic, I. (1999). Dynamical analysis and control of micro-cantilevers, *Automatica,* Vol. 35 , pp. 1663–1670.

Barry, E.; DeMartini, B. E.; Butterfield, E. ; Moehlis, J. & Turner, K. (2007). Chaos for a Microelectromechanical Oscillator Governed by the Nonlinear Mathieu Equation, *Journal of Microelectromechanical Systems*, Vol. 16, pp. 1314–1323.

Basso, M.; Giarrk, L.; Dahleh, M. & Mezic, I. (1998). Numerical analysis of complex dynamics in atomic force microscopes, *Proc. IEEE Int. Conf. Control Appl.*

Burnham, N.A. ; Kulik, A.J. ; Gremaud, G. & Briggs, G.A.D. (1995). Nanosubharmonics: The dynamics of small nonlinear contacts, *Phys. Rev. Lett.*, Vol. 74, pp. 5092–5059.

Calvo, O. (1998), Fuzzy control of chaos, *International Journal of Bifurcation and Chaos*, Vol. 8, No. 8, pp 1743–1747.

Chacon, R. (1999). General results on chaos suppression for biharmonically driven dissipative systems. *Phys Lett A*; 257, pp. 293–300.

Endo, T. & Chua, L. O. (1991). Synchronization of chaos in phase-locked loops, *IEEE Trans. Circuits Syst.*, Vol. 38, pp. 1580-1588.

Garcia, R.; Tamayo, J. & San Paulo, A. (1999). Phase contrast and surface energy hysteresis in tapping mode scanning force microscopy, *Surface Interface Anal* 27, pp.312–316.

Haghighi, H.S. & Markazi, A.H.D. (2010), Chaos prediction and control in MEMS resonators, *Commun Nonlinear Sci Numer Simulat*, Vol. 15, pp. 3091–3099.

Hansma, P.K.; Elings, V.B.; Marti, O. & Bracker, C.E. (1988). Scanning tunneling microscopy and atomic force microscopy: Application to biology and technology, *Science*, Vol. 242 , pp. 209-242.

Harley, J.A.; Chow, E.M. & Kenny, T.W. (1998). Design of resonant beam transducers: An axial force probe for atomic force microscopy, *In Micro-Electro-Mechanical Systems: ASME Intl. ME Congress and Exposition*, pp 274-252, Anaheim, Ca.

Jamitzky, F.; Stark, M.; Bunk, W.; Heckl, W.M. & Stark, R.W. (2006). Chaos in dynamic atomic force microscopy, *Nanotechnology*, Vol. 17 pp. 213–220.

Kennedy, M. P. (1993). Three steps to chaos, Part I: Evolution, Part II: A Chua's circuit primer, *IEEE Trans. Circuits Syst*. I, Vol. 40, No.10, pp.640-656.

Lin, L.; Howe, R. & Pissano, A.P. (1998). Microelectromechanical filters for signal processing, *J Microelectromech. Syst*. Vol. 7, No.3, pp. 286–294.

Liu, S; Davidson, A; & Lin, Q. (2004). Simulation studies on nonlinear dynamics and chaos in a MEMS cantilever control system, *Journal of Micromechanics and Microengineer*ing,Vol. 14, pp. 1064–1073.

Logeeswaran, V.J.; Tay, F.E.H.; Chan, M.L.; Chau, F.S. & Liang, Y.C. (2002). *Proceedings of the DTIP 2002 on A 2f Method for the Measurement of Resonant Frequency and Q-factor of Micromechanical Transducers*, ,pp. 584–590, Cannes, May 2002.

Luo, A. & Wang Fei-Yue. (2002). Chaotic motion in a micro-electro-mechanical system with non-linearity from capacitors, *Commun Nonlinear Sci Numer Simul*, Vol. 7, pp. 31–49.

Melnikov, VK. (1963). On the stability of the center for time periodic perturbations. *Trans Moscow Math Soc*,12, pp. 1–57.

Mestrom, R.M.C.; Fey, R.H.B.; van Beek, J.T.M.; Phan, K.L. & Nijmeijer, H. (2007). Modeling the dynamics of a MEMS resonator: Simulations and experiments, *Sens. Actuators A*, Vol. 142 ,pp. 306-315.

Moon, F. C. & Holmes, P. A magnetoelastic strange attractor, *J Sound Vib.*, Vol. 65, No. 2, pp. 285–296.

Nayfeh, A.H.; Younis, M.I.; Abdel-Rahman, E. (2007). Dynamic pull-in phenomenon in MEMS resonators, *Nonlinear Dynamics*,Vol. 48,pp. 153-63.

Poursamad, A. & Davaie-Markazi, A.H. (2009-a). Robust adaptive fuzzy control of unknown chaotic systems, *Applied Soft Computing*, Vol. 9, pp. 970–976.

Poursamad, A. & Markazi, A.H.D. (2009-b) Adaptive fuzzy sliding-mode control for multi-input multi-output chaotic systems, *Chaos, Solitons Fractals*, Vol. 42, pp. 3100–3109.

Roukes, M. (2001). Nanoelectromechanical systems face the future, *Phys.World,* Vol. 14 , pp. 25.

Wang, Y.C.; Adams, S.G.; Thorp, J.S.; MacDonald, N.C.; Hartwell, P. & Bertsch, F. (1998). Chaos in MEMS, parameter estimation and its potential application, *IEEE Trans. Circuits Syst. I*, Vol. 45, pp. 1013–1020.

Xie, H. & Fedder, G. (2002). Vertical comb-finger capacitive actuation and sensing for coms-MEMS, *Sens. Actuators A*, Vol. 95 , pp. 212–221.

Yagasaki, K. (2007), Bifurcations and chaos in vibrating microcantilevers of tapping mode atomic force microscopy, *Journal of Non-Linear Mechanics*, Vol. 42, pp. 658 – 672.

Younis, M. I. & Nayfeh, A. H. (2003). A Study of the Nonlinear Response of a Resonant Microbeam to an Electric Actuation, *Nonlinear Dynamics*, Vol. 31, No. 1 pp. 91–117.
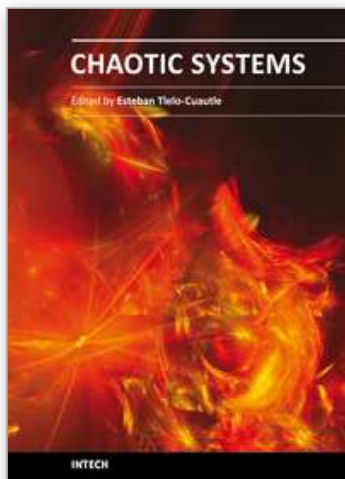
Chaotic Systems

Edited by Prof. Esteban Tlelo-Cuautle

This book presents a collection of major developments in chaos systems covering aspects on chaotic behavioral modeling and simulation, control and synchronization of chaos systems, and applications like secure communications. It is a good source to acquire recent knowledge and ideas for future research on chaos systems and to develop experiments applied to real life problems. That way, this book is very interesting for students, academia and industry since the collected chapters provide a rich cocktail while balancing theory and applications.

How to reference

In order to correctly reference this scholarly work, feel free to copy and paste the following:

Amir Hossein Davaie-Markazi and Hossein Sohanian-Haghighi (2011). Chaos Analysis and Control in AFM and MEMS Resonators, Chaotic Systems, Prof. Esteban Tlelo-Cuautle (Ed.), ISBN: 978-953-307-564-8, InTech, Available from: http://www.intechopen.com/books/chaotic-systems/chaos-analysis-and-control-in-afm-and-mems-resonators

INTECH
open science | open minds